NIH Public Access
Author Manuscript
*Biochemistry*. Author manuscript; available in PMC 2010 September 1.

Published in final edited form as:
*Biochemistry*. 2009 September 1; 48(34): 8129. doi:10.1021/bi9008648.

# Structures of the phosphorylated and $VO_3$-bound 2H-phosphatase domain of Sts-2

**Yunting Chen**[1], **Jean Jakoncic**[2], **Kathlyn A. Parker**[3], **Nick Carpino**[4], and **Nicolas Nassar**[1,*]

[1]Department of Physiology and Biophysics, Stony Brook University, Stony Brook, NY 11794

[2]Brookhaven National Laboratory, National Synchrotron Light Source Bldg 725, Upton, NY 11973

[3]Department of Chemistry, Stony Brook University, Stony Brook, NY 11794

[4]Department of Molecular Genetics and Microbiology, Stony Brook University, Stony Brook, NY 11794

## Abstract

The C-terminal domain of the suppressor of T cell receptor (TCR) signaling 1 and 2 (Sts-1 and -2) proteins has homology to the 2H-phosphatase family of enzymes. The phosphatase activity of the correspondent Sts-1 domain, Sts-$1_{PGM}$, is key for its ability to negatively regulate the signaling of membrane-bound receptors including TCR and the epidermal growth factor receptor (EGFR). A nucleophilic histidine, which is transiently phosphorylated during the phosphatase reaction, is essential for the activity. Here we present the crystal structure of Sts-$2_{PGM}$ in the phosphorylated active form and bound to $VO_3$, which represent structures of an intermediate and of a transition state analogue along the path of the dephosphorylation reaction. In the former structure, the proposed nucleophilic His366 is the only phoshorylated residue and is stabilized by several interactions with conserved basic residues within the active site. In the latter structure, the vanadium atom sits in the middle of a trigonal bipyramid formed by the three oxygen atoms of the $VO_3$ molecule, atom NE2 of His366, and an apical water molecule $W_a$. The V-NE2 bond length (2.25 Å) suggests that $VO_3$ is not covalently attached to His366 and that the reaction mechanism is partially associative. The two structures also suggest a role for Glu476 in activating a uniquely positioned water molecule. In both structures, the conformation of the active site is remarkably similar to the one seen in apo-Sts-$2_{PGM}$ suggesting that the spatial arrangement of the catalytic residues does not change during the dephosphorylation reaction.

### Keywords

Suppressor of T cell signaling proteins; Sts-1; Sts-2; EPPase; PGM; 2H-phosphatase; X-ray crystallography; phosphoramidate; vanadium oxide; phosphatase mechanism; phosphorylated intermediate; transition state

---

The 2H-phosphatase superfamily of enzymes, also referred to as the phosphoglycerate mutase (PGM) superfamily, is so called because the majority of its members are phosphatases that use two catalytic histidine residues to dephosphorylate substrates (1,2). The first His residue belongs to the ‘RHGE’ signature motif that is conserved among family members and is the nucleophilic residue during catalysis. The second His residue together with two conserved Arg residues are scattered in the primary sequence, complete the active site, and give it a basic

*CORRESPONDING AUTHOR Nicolas Nassar, Department of Physiology and Biophysics, Basic Sciences Tower, Stony Brook University, Stony Brook, NY 11794-8661. Tel: 631-444-3521, FAX: 631-444-3432; nicolas.nassar@sunysb.edu.

NIH-PA Author Manuscript
NIH-PA Author Manuscript
NIH-PA Author Manuscript

NIH-PA Author Manuscript

NIH-PA Author Manuscript

NIH-PA Author Manuscript

potential character that attracts and stabilizes phosphorylated substrates. Outside the His and Arg residues, the primary sequence of these enzymes shows little conservation. Despite the low sequence homology, the overall tertiary fold of these enzymes is overall maintained; more importantly the structure of the active site is highly conserved. Family members include the diverse acid phosphatases (AcPs), the cofactor dependent phosphoglycerate mutase (dPGM), the fructose 2,6-bisphosphatase (F2,6BP), the TIGAR protein (3), the Sts proteins (4), and many others. The diversity among family members is reflected in substrate diversity and specificity: substrates range from small-phosphorylated molecules to phospho-proteins, and some enzymes are very specific (F2,6BP) while others are promiscuous (AcPs).

The dephosphorylation reaction is believed to be a two-step reaction (Scheme) (5). In the first step, the nucleophilic His of the 'RHGE' signature motif attacks the phosphorus atom of the substrate resulting in the transient transfer of the phosphate to the His and the release of the dephosphorylated substrate. In the second step, the phospho-His is hydrolyzed by an activated water molecule and the enzyme returns to its resting state. The second His and the Arg residues are believed to stabilize the negative charges that appear on the structure of the transition state species. The nucleophilic attacking water molecule is activated by general base catalysis usually by the side chain carboxylate of an Asp or Glu residue (6,7). As in many phospho-transferases, determining the crystal structures of family members in the presence of phosphate and phosphate-like species including vanadate and tungstate has been very useful in understanding the reaction mechanism and highlighting the catalytic amino acids and water molecules. However, except for the structures of the phospho-histidine activated form of the *Escherichia coli* dPGM (8) and human bisphosphoglycerate mutase (BPGM) (9), little is known about the phospho-histidine transient intermediate state of the 2H-phosphatases. More generally, there are few high-resolution structures of phosphohistidine-containing proteins, those of the *Drosophila* and *Dictyostelium* nucleoside diphosphate (NDP) kinase (10), the pig heart GTP-specific succinyl-CoA synthetase (11), and the *Bacillus subtilis* histidine-containing protein (HPr) (12) being the exception.

To shed additional light on the dephosphorylation reaction carried out by the 2H-phosphatases, we focused on determining the structures of the transition states for hydrolysis of the Sts proteins. Sts-1 and -2 proteins are multidomain proteins that contain a C-terminal 2H-phosphatase homology domain (13-16). Functionally, they play an important role in downregulating the activity of the TCR. Despite the sequence homology between the 2H-phosphatase domains of the two isoforms, the phosphatase activity of Sts-$2_{PGM}$ is by far the weaker one despite conservation of all catalytic residues. We have recently determined the crystal structure of Sts-$1_{PGM}$ and Sts-$2_{PGM}$ alone or in complex with phosphate and tungstate (4,17). Here we present the crystal structures of Sts-$2_{PGM}$ in the active phosphorylated state and bound to vanadium oxide ($VO_3$).

## Experimental Methods

### Protein Preparation

The 2H-phosphatase domain of mouse Sts-2 (residues 354-624) was cloned and purified as described previously (17).

### Phosphoramidate Synthesis

The synthesis of dipotassium phosphoramidate was performed by the method of Wei and Matthews (18). A stock solution of 0.5 M was prepared in water.

NIH-PA Author Manuscript

NIH-PA Author Manuscript

NIH-PA Author Manuscript

### Protein Crystallization

Crystals of Sts-$2_{PGM}$ in complex with vanadium oxide were grown at 20 °C by mixing 3 μL of 20 mg/mL Sts-$2_{PGM}$ (in 20 mM HEPES, 150 mM NaCl, pH = 7.5) and 3 μL of a reservoir solution. The reservoir consisted of 18 - 20% (w/v) polyethylene glycol-4000 (PEG4000), 0.2 M lithium sulfate, 0.1 M Tris-acetate pH = 8.0, 2 mM sodium vanadium oxide (Alfa Aesar, MA), and 2 mM L-tyrosine. To ensure the removal and conversion of high order vanadate complexes to monomers, the vanadate stock solution was heated before usage until it became colorless. Crystals belonged to space group $P2_12_12_1$ (a = 77.4 Å, b = 114.8 Å, c = 120.9 Å) with two dimers in the asymmetric unit. Crystals of phosphorylated Sts-$2_{PGM}$ were obtained by soaking crystals of apo-Sts-$2_{PGM}$ grown as described previously (17) into cryoprotectant solutions supplied with 20 mM phosphoramidate for 15 minutes before cooling in liquid nitrogen.

### Data Collection, Structure Determination, and Refinement

All diffraction intensities were collected at 100 K on beam line X6A at the National Synchrotron Laboratory Source (NSLS), Brookhaven, on a 2k × 2k CCD detector (ADSC), at a wavelength of 0.9796 Å, integrated and scaled with the HKL2000 package (19).

The structures were solved by the difference Fourier technique using the coordinates of apo-Sts-$2_{PGM}$ (PDB entry 3D4I). The models were refined in REFMAC (20) with one final round of TLS (21), visualized and manually rebuilt in the program O (22). Water molecules were added in difference Fourier electron density maps visualized at 4σ when the $R_{free}$ (23) was < 32%. The $VO_3^-$, phospho-His366, and metal ions were added at the final stages of the refinement. Each phosphate group and its attached metal ion were assigned the same occupancy, which was manually refined in REFMAC until the residual density of this group disappeared from a difference Fourier map (±2σ). Stereochemistry was checked with the program PROCHECK (24). Table 1 summarizes statistics on data collection and model refinement. Coordinates of the phosphorylated and $VO_3$-bound forms of Sts-$2_{PGM}$ have been deposited at the PDB databank.

## RESULTS

### Structure of the phosphohistidine active form of Sts-$2_{PGM}$

To shed light on the structure of the phospho-histidine intermediate, we incubated Sts-$2_{PGM}$ crystals with cryoprotectant solutions to which phosphoramidate was added prior to cooling them in liquid nitrogen. Phosphoramidate ($NH_2PO_3^{2-}$) is a phosphate donor that was successfully used to phosphorylate the nucleophilic histidine of the *Staphylococcus aureus* phosphocarrier protein HPr (25) and of the NDP kinase (10). Inspection of the diffraction quality showed that the best results were obtained when the crystals were incubated with 20 mM of the phosphodonor phosphoramidate for 10 to 15 minutes. Longer incubations resulted in the loss of the diffraction power of the crystals while shorter incubation times resulted in a lower degree of phosphorylation. A difference Fourier electron density map calculated to 2.05 Å resolution with phases deduced from the apo-Sts-$2_{PGM}$ model (17) clearly showed peaks at higher than 5σ close to His366 in three of the four monomers occupying the asymmetric unit (Figure 1A). The residual electron density could only be interpreted as that of a (-$PO_3$) moiety covalently attached to atom NE2 of His366. Inspection of the electron density map showed that His366 was the only residue phosphorylated by phosphoramidate. Refinement against the experimental diffraction data showed that the occupancy of the phosphate group is monomer dependent and varies between 0.50 and 0.70. This result suggests that the phosphoramidate on average phosphorylated 60% of the His366 present in the crystal. An extra electron density was also found close to each phosphate group. The chemical nature of each extra density is unknown but based on the refined temperature factor and the residual difference Fourier density

NIH-PA Author Manuscript

NIH-PA Author Manuscript

NIH-PA Author Manuscript

it is consistent with a sodium ion and not a lithium or potassium ion. However, the $Na^+$-ions in our structure are on average 2.0 Å from the solvent exposed phosphate oxygen (Figure 1A), which is shorter than the average 2.4 Å $Na^+$-O distances reported in the literature (26). For all purposes, $Na^+$ will be used to explain the extra electron density in the vicinity of each phosphate.

Figure 1A illustrates how the phospho-His366 is stabilized in the active site. The phosphorylation of His366 did not disturb the overall structure of Sts-$2_{PGM}$ as seen by the low rms deviation of 0.4 Å calculated after superposition of the apo-structure. The structure of the active site, including the interactions made by the catalytic residues, is also remarkably unperturbed (Figure 1B). As in the apo-structure, the imidazole ring is held in place by steric interactions involving Arg365 and Arg448 on one side of the ring and Arg369 and His551 on the other. In addition, ND1 of phospho-His366 is making a hydrogen bond with the main chain carbonyl group of Gly367 suggesting that ND1 is protonated. This hydrogen bond is consistent with a deprotonated NE2 capable of a nucleophilic attack on the phosphorus atom of the phosphoramidate. The covalently attached (-$PO_3$) group replaces three water molecules that were within hydrogen bond distances from His366 in the apo-structure. The average P-NE2 covalent-bond distance (1.78 Å) is consistent with analogous distances observed in high-resolution crystal structures (8, 9). The (-$PO_3$) group is stabilized by hydrogen bond interactions with the side chains of Arg365, Arg369, Arg448, and His551 and the main chain amino group of Ser552. These residues are conserved in Sts-$1_{PGM}$ and other 2H-phosphatases suggesting that all family members share the described mode of stabilization of the phospho-histidine moiety. Mutation of the equivalent residues in Sts-1 dramatically reduced its catalytic activity (4) consistent with their role in stabilizing the structure of the intermediate.

In two monomers belonging to two independent dimers, a water molecule (labeled W in Figure 1A) is found 5 Å from the phosphorus atom but is absent from the two other monomers. This water molecule is not perfectly in-line with the P-NE2 bond but is situated such that the W-P-NE2 angle is 142°. It is stabilized by hydrogen bond interactions with the main chain amino and side chain hydroxyl groups of Ser553 (2.90 and 3.50 Å, respectively) and the carboxylic group of Glu476 (2.60 Å), the proposed general base of the dephosphorylation reaction. Based on its relative closeness to the phosphorus atom and relative orientation, it is likely that this water molecule is the nucleophilic attacking water molecule responsible for dephosphorylating phospho-His366 in the second step of the enzymatic reaction. In such a scenario, Glu476 activates the water molecule W during the nucleophilic attack on phospho-His366 and becomes protonated. In support of this hypothesis, the carboxylic group of Glu476 is within hydrogen bond distances from the hydroxyl group of Ser553 (2.6 Å) and the main chain amino group of Trp477 (2.8 Å) suggesting that it is deprotonated and therefore negatively charged. Interestingly, a similarly situated water molecule was found in tungstate-bound and in apo-Sts-$2_{PGM}$ and was also proposed to be the nucleophilic attacking water (17).

The structure of phospho-Sts-$2_{PGM}$ allows the comparison with the structures of the activated form of *E. coli* dPGM (8) and human BPGM (9), which are partially phosphorylated on His10 and His11 respectively, the equivalent of His366. In dPGM, the covalently attached (-$PO_3$) group makes additional interactions with the enzyme active site including hydrogen bonds with the proposed general base Glu88 (Glu476 in Sts-$2_{PGM}$), with Asn16 (Asn372 in Sts-$2_{PGM}$), and an adjacent water molecule. In Sts-$2_{PGM}$, the closest hydrogen donor or acceptor atom of Asn372 and Glu476 are 4.8 and 3.5 Å, respectively from phospho-His366. It is not clear whether these structural differences imply subtle differences between the two enzymes in the second step of the hydrolysis reaction or whether they might reflect the percentage in histidine phosphorylation (28% in dPGM versus ~60% in Sts-$2_{PGM}$) between the two enzymes, the difference in crystal packing, or the manner in which the phosphorylated enzymes were prepared: Sts-$2_{PGM}$ was phosphorylated by diffusing phosphoramidate in the crystal while

NIH-PA Author Manuscript

NIH-PA Author Manuscript

NIH-PA Author Manuscript

dPGM was purified as a phosphorylated recombinant protein (8). In BPGM, the interactions between the conserved catalytic residues and the covalently attached (-$PO_3$) are all present except for the interaction with the equivalent of Arg369. Subtle differences are also observed but these could be due to the presence of the substrate and product in the active site of BPGM, which create a mixture of states in the crystal (9).

Our phosphoramidate data thus show that it is possible to stabilize the structure of the phosphorylated enzyme intermediate on the path for substrate dephosphorylation. This reinforces our previous observation that Sts-$2_{PGM}$ has intrinsic phosphatase activity (4,17). They also show that during catalysis the substrate's phosphate is transferred to the conserved histidine of the 'RHGE' motif highlighting the importance of this motif and its conservation among 2H-phosphatase family members.

## Structure of the $VO_3$-bound Sts-$2_{PGM}$

To gain more insight into the phosphatase reaction catalyzed by Sts-$2_{PGM}$, we crystallized Sts-$2_{PGM}$ in the presence of activated sodium vanadium oxide and L-tyrosine and solved the crystal structure of this complex. We added L-Tyr and $VO_3$ to the crystallization mixture because in a few instances the phosphate mimic vanadium oxide was found to covalently mediate the interaction between an enzyme and its substrate, thereby revealing the structure of transition state mimics (27). The electron density map calculated to 1.87 Å resolution clearly shows a planar electron density close to His366 and perpendicular to its imidazole ring in the active site of every Sts-$2_{PGM}$ monomer in the asymmetric unit. We interpreted this extra density as that of a $VO_3$ molecule. A difference anomalous electron density map showed peaks at higher than 4 sigmas that superposed on the vanadium atoms confirming our hypothesis (Figure 2A). A water molecule was found apical to the $VO_3$ molecule in three monomers but was missing in the fourth. The active site of this monomer is characterized by higher temperature factors. We could not locate any L-Tyr in the vicinity of the $VO_3$ moiety or elsewhere in the electron density map. To check that the extra electron density close to His366 is that of $VO_3$ and an apical water molecule and not that of a contaminant vanadate ($VO_4$) molecule, we refined the latter in the electron density map. The appearance of positive and negative peaks in the calculated difference Fourier map confirms that the $VO_3$/apical water molecule explains better the diffraction data.

As with the tungstate-and phosphate-bound structures (17), the binding of the $VO_3$ molecule did not disturb the structure of the active site. Illustrated in Figure 2B are the basic structural features of the $VO_3$ molecule along with primary interactions involving key residues in the enzyme active site. As seen in the figure, the pentavalently coordinated vanadium atom sits in the middle of a slightly distorted trigonal bipyramid formed by the three equatorial oxyanion atoms, the apical water molecule, and NE2 of His366. The apical water molecule ($W_a$) is not perfectly in line with the V and NE2 atoms. As a consequence, the $W_a$-V-NE2 angle (average of 160° ± 1.5°) deviates by 20° from the expected 180°. The axial bond distances are slightly elongated relative to those in the equatorial plane resulting in a slightly distorted trigonal bipyramid; whereas the average V-O distance is 1.90 Å, the average V-NE2 and V-$W_a$ distances are 2.25 and 2.1 Å, respectively. These distances are within the range of analogous distances reported in the literature for enzyme complexes with vanadate. For comparison, the average V-O bond distance of 1.9 Å observed here is similar to the 2.1 Å and 1.8 Å reported for the 2-Keto-3-deoxy-D-glycero-D-galactonononate-9-phosphate phosphatase (28) and for the tyrosyl-DNA phosphodiesterase (Tdp1) (29), respectively, but longer than the 1.65 Å observed with the chloroperoxidase (30). The average V-NE2 bond distance of 2.25 Å is also consistent with the analogous distance of 2.25 Å found in the chloroperoxidase (30), or 2.11 Å in the vanadium-dependent haloperoxidase (31), or Tdp1 (29) but longer than the 2.0 Å bond reported for the rat acid phosphatase (32). The V-NE2 distance reported here is also similar to

NIH-PA Author Manuscript

NIH-PA Author Manuscript

NIH-PA Author Manuscript

P-NE2 bond distances found experimentally or by molecular dynamics simulations between the planar metaphosphate anion $PO_3^-$ and nucleophilic histidines (33,34). The finding that the V-NE2 distance is larger than 2.0 Å suggests that the $VO_3$ molecule is not covalently bound to Sts-$2_{PGM}$. Consequently, the vanadium atom is situated further away from NE2 of His366 than the phosphorus atom in phospho-His366 (Figure 2C). In addition to the apical water molecule, an extra density was found close to oxyanion O1, which we interpret as that of a $Na^+$ ion. The likely role of this sodium ion is to neutralize the negative charge of the $VO_3$. The distances between this ion and O1 of the $VO_3$ molecule vary between 1.5 and 1.8 Å with an average of 1.63 Å.

As expected, the side chain of the active site basic residues Arg369, Arg448, Arg462, and His551 are within hydrogen bond distances of the $VO_3$ molecule. In addition to these conserved residues, the hydroxyl and the main chain amino groups of Ser552 are within hydrogen bond distances of the $VO_3$ molecule. The coordination of the $VO_3$ molecule in the active site is very similar to that of the tungstate (17) with the exception of Arg365 of the 'RHGE' signature motif, which interacts with the tungstate but not the $VO_3$ molecule. This dissimilarity could be due to the size difference between the two inorganic molecules or to the difference in their proximity to atom NE2 of His366. The apical water molecule ($W_a$) is not within a hydrogen bond distance from any active site residue but is close to the Na+ ion. The closest active site residues to the apical water are Arg369 and Glu476. The distance to the guanidinium group of the former is ~3.9 Å while the distance to the carboxylic group of the latter is monomer-dependent and varies between 3.8 and 4.5 Å. The proximity of Glu476 to the apical water molecule is consistent with its role as a general base that activates the nucleophilic water molecule by deprotonating it.

Nucleophilic substitution at phosphorus occurs at each step of the dephosphorylation reaction catalyzed by 2H-phosphatases, i.e. during the phosphate transfer from the substrate to the enzyme and when the enzyme is dephosphorylated to return to its resting state. Since $AlF_3$, $AlF_4^-$ or $VO_3$ are often used to mimic the transition state in phosphoryl transfer reactions, it is likely that the $VO_3$-bound structure described here mimics the structure of the transition state for the dephosphorylation reaction catalyzed by Sts-$2_{PGM}$. Thus, $W_a$ mimics the oxygen of the leaving group in the first half of the reaction and the nucleophilic attacking water in the second half of the reaction, respectively. Interestingly, a water molecule (labeled W in Figure 2B) is also present in the $VO_3$-bound structure at the site we previously predicted to be occupied by the nucleophilic attacking water in the apo-and tungstate-bound structures suggesting that as soon as the nucleophilic attack on the phosphate takes place, this site is reoccupied by another water molecule from the solvent.

## DISCUSSION

We previously suggested that the tungstate-and the phosphate-bound structures of Sts-$2_{PGM}$ mimic the structures of the enzyme just before the nucleophilic attack on the phosphorylated substrate and that of the inorganic phosphate-bound product, respectively (17). The structures of the phosphorylated and the $VO_3$-bound protein presented here constitute additional molecular snapshots along the path of the phosphatase reaction catalyzed by Sts-$2_{PGM}$ and probably other 2H-phosphatases. They provide evidence that the transfer of phosphate from the substrate to His366 occurs by an in line reaction that is partially associative. Assuming that the Sts-$2_{PGM}$-$VO_3$-$W_a$ structure is a good mimic of the phosphate trigonal bipyramidal transition state and assuming that $W_a$ mimics the oxygen of the leaving group, the axial bond lengths of 2.25 and 2.1 Å in this complex yield a mechanism for Sts-2 phosphatase that is 13.5% associative from the entering group and 24% associative from the leaving group. The bond orders here are similar to previously reported numbers for the myosin ATPase, BPGM phosphatase, and β-phosphoglucomutase (9,35,36).

NIH-PA Author Manuscript

NIH-PA Author Manuscript

NIH-PA Author Manuscript

Our structural data also confirm previously published findings regarding Sts-$2_{PGM}$. Four major conclusions can be deduced from our work. Firstly, the structural data are consistent with a functional 2H-phosphatase domain for Sts-2. The conserved catalytic His and Arg residues adopt conformations in the active site that are similar to their counterparts in other active 2H-phosphatases including the more active and homologous Sts-$1_{PGM}$. Secondly, the catalytic residues are involved in interactions consistent with their predicted role. Specifically, His366 of the conserved 'RHGE' signature motif can be phosphorylated and is the closest residue to the tungstate and $VO_3$ moieties, consistent with its role as the attacking nucleophile. In addition, the conserved Arg365, Arg448, and His551 interact tightly with the tungstate, $VO_3$ and phospho-His366, in line with their role in stabilizing the negative charge buildup during catalysis. Thirdly, the apo-, phosphorylated, tungstate-and $VO_3$-bound structures of Sts-$2_{PGM}$ highlight a water molecule that is present at the same location in all structures as a candidate for the nucleophilic attack on phospho-His366. Among other residues, Glu476, the proposed general base stabilizes this water molecule. We propose that Glu476 deprotonates the nucleophilic water molecule to generate a hydroxyl group that attacks the phosphorus atom of the phospho-histidine. Protonated Glu476 loses its proton to the leaving group in the next cycle either directly or through an active site water molecule (34). Fourthly, superposition of the various Sts-$2_{PGM}$ coordinates indicates that the structure of the active site and its surrounding loops does not change regardless of the state of the enzyme or the nature of the bound-molecule. The rigidity of the active site suggests that only subtle movements of side chain residues are necessary for activity. This picture is to be contrasted with BPGM where parts of the active site surrounding loops close on the active site upon binding of the 2,3-bisphosphoglycerate (BPG) substrate. The nucleophilic histidine also rotates by 20° and moves by 0.5 Å toward the BPG (9). Other phosphatases like the Cys-based protein tyrosine phosphatases (PTPs) including PTP-1B also witness large loop movements during hydrolysis (37,38). Whether this observed rigidity is inherent to Sts-2 active site or is due to crystal packing forces remains to be established. That the asymmetric unit is occupied by four Sts-$2_{PGM}$ monomers that differ in their crystal packing favors the idea of a rigid active site. However, it is also possible that some of the active site loops will change conformation in the presence of a substrate molecule.

## Acknowledgments

We thank Ben Sondgeroth for expert technical assistance and Vivian Stojanoff for help with data collection at X6A.

FUNDING: Research in NN's laboratory is supported in part by grants from the NIH (CA-115611) and DOD (NF060060). Research in NC's laboratory is supported by grants from The Arthritis Foundation (LI07), NIH-NIAID (R21AI075176), and The National Multiple Sclerosis Society through a Collaborative MS Research Center Award (CA1044A1). Research carried out at X6A beam line, National Synchrotron Light Source, Brookhaven National Laboratory, is supported by the U.S. Department of Energy under contract # DE-AC02-98CH10886. X6A is funded by NIH/NIGMS under agreement Y1 GM-0080-03.

## References

1. Rigden DJ. The histidine phosphatase superfamily: structure and function. Biochem J 2008;409:333–348. [PubMed: 18092946]
2. Jedrzejas MJ. Structure, function, and evolution of phosphoglycerate mutases: comparison with fructose-2,6-bisphosphatase, acid phosphatase, and alkaline phosphatase. Prog Biophys Mol Biol 2000;73:263–287. [PubMed: 10958932]
3. Bensaad K, Tsuruta A, Selak MA, Vidal MN, Nakano K, Bartrons R, Gottlieb E, Vousden KH. TIGAR, a p53-inducible regulator of glycolysis and apoptosis. Cell 2006;126:107–120. [PubMed: 16839880]
4. Mikhailik A, Ford B, Keller J, Chen Y, Nassar N, Carpino N. A phosphatase activity of Sts-1 contributes to the suppression of TCR signaling. Mol Cell 2007;27:486–497. [PubMed: 17679096]
5. Van Etten RL. Human prostatic acid phosphatase: a histidine phosphatase. Ann N Y Acad Sci 1982;390:27–51. [PubMed: 6124201]

NIH-PA Author Manuscript

NIH-PA Author Manuscript

NIH-PA Author Manuscript


6. Lin K, Li L, Correia JJ, Pilkis SJ. Glu327 is part of a catalytic triad in rat liver fructose-2,6-bisphosphatase. J Biol Chem 1992;267:6556–6562. [PubMed: 1313012]
7. Ostanin K, Van Etten RL. Asp304 of Escherichia coli acid phosphatase is involved in leaving group protonation. J Biol Chem 1993;268:20778–20784. [PubMed: 8407904]
8. Bond CS, White MF, Hunter WN. High resolution structure of the phosphohistidine-activated form of Escherichia coli cofactor-dependent phosphoglycerate mutase. J Biol Chem 2001;276:3247–3253. [PubMed: 11038361]
9. Wang Y, Liu L, Wei Z, Cheng Z, Lin Y, Gong W. Seeing the process of histidine phosphorylation in human bisphosphoglycerate mutase. J Biol Chem 2006;281:39642–39648. [PubMed: 17052986]
10. Morera S, Chiadmi M, LeBras G, Lascu I, Janin J. Mechanism of phosphate transfer by nucleoside diphosphate kinase: X-ray structures of the phosphohistidine intermediate of the enzymes from Drosophila and Dictyostelium. Biochemistry 1995;34:11062–11070. [PubMed: 7669763]
11. Fraser ME, James MN, Bridger WA, Wolodko WT. Phosphorylated and dephosphorylated structures of pig heart, GTP-specific succinyl-CoA synthetase. J Mol Biol 2000;299:1325–1339. [PubMed: 10873456]
12. Jones BE, Rajagopal P, Klevit RE. Phosphorylation on histidine is accompanied by localized structural changes in the phosphocarrier protein, HPr from Bacillus subtilis. Protein Sci 1997;6:2107–2119. [PubMed: 9336834]
13. Carpino N, Kobayashi R, Zang H, Takahashi Y, Jou ST, Feng J, Nakajima H, Ihle JN. Identification, cDNA cloning, and targeted deletion of p70, a novel, ubiquitously expressed SH3 domain-containing protein. Mol Cell Biol 2002;22:7491–7500. [PubMed: 12370296]
14. Carpino N, Turner S, Mekala D, Takahashi Y, Zang H, Geiger TL, Doherty P, Ihle JN. Regulation of ZAP-70 activation and TCR signaling by two related proteins, Sts-1 and Sts-2. Immunity 2004;20:37–46. [PubMed: 14738763]
15. Kowanetz K, Crosetto N, Haglund K, Schmidt MH, Heldin CH, Dikic I. Suppressors of T-cell receptor signaling Sts-1 and Sts-2 bind to Cbl and inhibit endocytosis of receptor tyrosine kinases. J Biol Chem 2004;279:32786–32795. [PubMed: 15159412]
16. Feshchenko EA, Smirnova EV, Swaminathan G, Teckchandani AM, Agrawal R, Band H, Zhang X, Annan RS, Carr SA, Tsygankov AY. TULA: an SH3-and UBA-containing protein that binds to c-Cbl and ubiquitin. Oncogene 2004;23:4690–4706. [PubMed: 15107835]
17. Chen Y, Jakoncic J, Carpino N, Nassar N. Structural and Functional Characterization of the 2H-Phosphatase Domain of Sts-2 Reveals an Acid-Dependent Phosphatase Activity (dagger). Biochemistry. 2009
18. Wei YF, Matthews HR. Identification of phosphohistidine in proteins and purification of protein-histidine kinases. Methods Enzymol 1991;200:388–414. [PubMed: 1956326]
19. Otwinowski Z, Borek D, Majewski W, Minor W. Multiparametric scaling of diffraction intensities. Acta Crystallogr A 2003;59:228–234. [PubMed: 12714773]
20. Murshudov GN, Vagin AA, Dodson EJ. Refinement of macromolecular structures by the maximum-likelihood method. Acta Crystallogr D Biol Crystallogr 1997;53:240–255. [PubMed: 15299926]
21. Winn MD, Isupov MN, Murshudov GN. Use of TLS parameters to model anisotropic displacements in macromolecular refinement. Acta Crystallogr D Biol Crystallogr 2001;57:122–133. [PubMed: 11134934]
22. Jones TA, Zou JY, Cowan SW, Kjeldgaard M. Improved methods for building protein models in electron density maps and the location of errors in these models. Acta Crystallogr A 1991;47(Pt 2): 110–119. [PubMed: 2025413]
23. Brünger AT. Free R value: a novel statistical quantity for assessing the accuracy of crystal structures. Nature 1992;355:472–475. [PubMed: 18481394]
24. Laskowski RA, Moss DS, Thornton JM. Main-chain bond lengths and bond angles in protein structures. J Mol Biol 1993;231:1049–1067. [PubMed: 8515464]
25. Gassner M, Stehlik D, Schrecker O, Hengstenberg W, Maurer W, Ruterjans H. The phosphoenolpyruvate-dependent phosphotransferase system of Staphylococcus aureus. 2. 1H and 31P-nuclear-magnetic-resonance studies on the phosphocarrier protein HPr, phosphohistidines and phosphorylated HPr. Eur J Biochem 1977;75:287–296. [PubMed: 862622]

NIH-PA Author Manuscript

NIH-PA Author Manuscript

NIH-PA Author Manuscript


26. Harding MM. Small revisions to predicted distances around metal sites in proteins. Acta Crystallogr D Biol Crystallogr 2006;62:678–682. [PubMed: 16699196]
27. Davies DR, Interthal H, Champoux JJ, Hol WG. Explorations of peptide and oligonucleotide binding sites of tyrosyl-DNA phosphodiesterase using vanadate complexes. J Med Chem 2004;47:829–837. [PubMed: 14761185]
28. Lu Z, Wang L, Dunaway-Mariano D, Allen KN. Structure-function analysis of 2-keto-3-deoxy-D-glycero-D-galactononononate-9-phosphate phosphatase defines specificity elements in type C0 haloalkanoate dehalogenase family members. J Biol Chem 2009;284:1224–1233. [PubMed: 18986982]
29. Davies DR, Interthal H, Champoux JJ, Hol WG. Insights into substrate binding and catalytic mechanism of human tyrosyl-DNA phosphodiesterase (Tdp1) from vanadate and tungstate-inhibited structures. J Mol Biol 2002;324:917–932. [PubMed: 12470949]
30. Messerschmidt A, Wever R. X-ray structure of a vanadium-containing enzyme: chloroperoxidase from the fungus Curvularia inaequalis. Proc Natl Acad Sci U S A 1996;93:392–396. [PubMed: 8552646]
31. Weyand M, Hecht H, Kiess M, Liaud M, Vilter H, Schomburg D. X-ray structure determination of a vanadium-dependent haloperoxidase from Ascophyllum nodosum at 2.0 A resolution. J Mol Biol 1999;293:595–611. [PubMed: 10543953]
32. Lindqvist Y, Schneider G, Vihko P. Crystal structures of rat acid phosphatase complexed with the transition-state analogs vanadate and molybdate. Implications for the reaction mechanism. Eur J Biochem 1994;221:139–142. [PubMed: 8168503]
33. de Macedo-Ribeiro S, Renirie R, Wever R, Messerschmidt A. Crystal structure of a trapped phosphate intermediate in vanadium apochloroperoxidase catalyzing a dephosphorylation reaction. Biochemistry 2008;47:929–934. [PubMed: 18163651]
34. Sharma S, Rauk A, Juffer AH. A DFT study on the formation of a phosphohistidine intermediate in prostatic acid phosphatase. J Am Chem Soc 2008;130:9708–9716. [PubMed: 18605729]
35. Mildvan AS. Mechanisms of signaling and related enzymes. Proteins 1997;29:401–416. [PubMed: 9408938]
36. Lahiri SD, Zhang G, Dunaway-Mariano D, Allen KN. The pentacovalent phosphorus intermediate of a phosphoryl transfer reaction. Science 2003;299:2067–2071. [PubMed: 12637673]
37. Denu JM, Dixon JE. Protein tyrosine phosphatases: mechanisms of catalysis and regulation. Curr Opin Chem Biol 1998;2:633–641. [PubMed: 9818190]
38. Barford D, Das AK, Egloff MP. The structure and mechanism of protein phosphatases: insights into catalysis and regulation. Annu Rev Biophys Biomol Struct 1998;27:133–164. [PubMed: 9646865]


## ABBREVIATIONS

| | |
|---|---|
| DTT | dithiothreitol |
| EPPase | ecdysteroid phosphate phosphatase |
| PGM | phosphoglycerate mutase |
| *p*NP | *para*-nitrophenol |
| *p*NPP | *para*-nitrophenylphosphate |
| PTP | protein tyrosine phosphatase |
| Sts | suppressor of T cell signaling |
| TCR | T cell receptor |

NIH-PA Author Manuscript
NIH-PA Author Manuscript
NIH-PA Author Manuscript



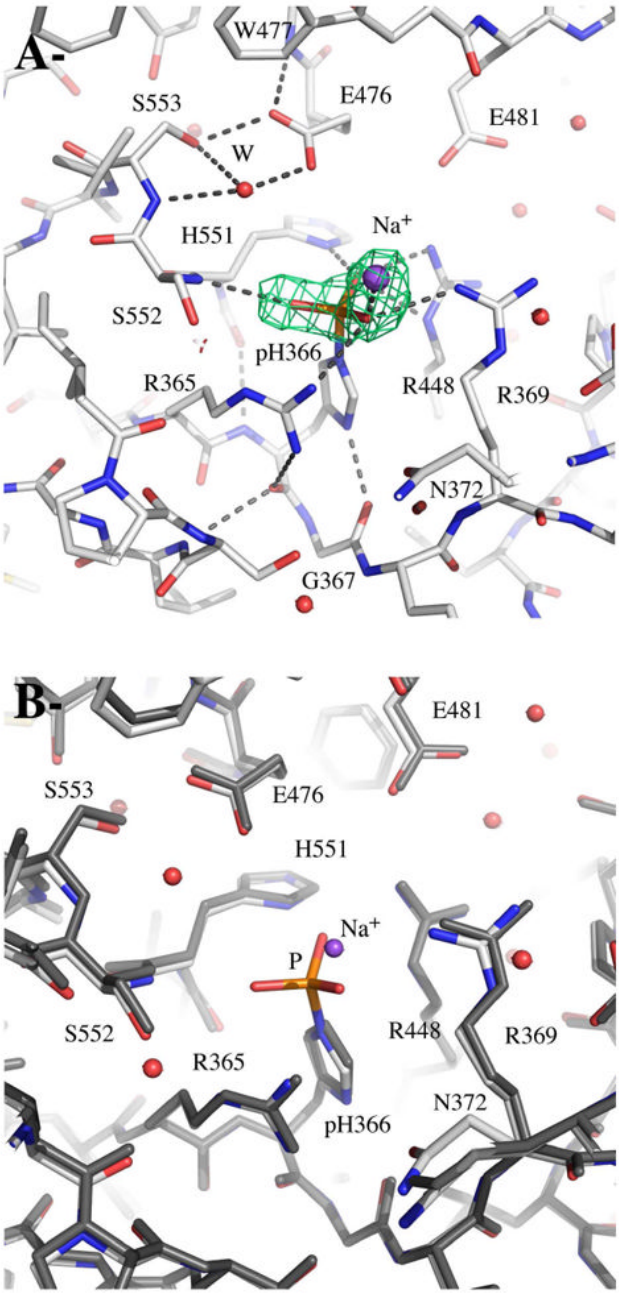


**Figure 1.**

Structure of phosphorylated active Sts-$2_{PGM}$. **A**- Interactions made by phospho-His366 (pH366) in the active site. Dotted lines represent putative hydrogen bond interactions. Superposed on the final model and shown at +3σ cutoff is the difference Fourier electron density map ($F_o - F_c$) (green mesh) calculated after removing all the phosphate groups and sodium ions from the refinement. The possible candidate for the nucleophilic water molecule is labeled with a W. **B**- Superposition of apo-Sts-$2_{PGM}$ (grey) and phosphorylated Sts-$2_{PGM}$. Active site residues are shown in ball-and-stick representation. For simplicity, water molecules are shown as red spheres for phosphorylated Sts-$2_{PGM}$ only. The $Na^+$-ion that coordinates the

covalently attached phosphate group is shown as a purple sphere. Figure prepared with PyMOL (http://pymol.sourceforge.net/).

NIH-PA Author Manuscript
NIH-PA Author Manuscript
NIH-PA Author Manuscript

NIH-PA Author Manuscript

NIH-PA Author Manuscript

NIH-PA Author Manuscript

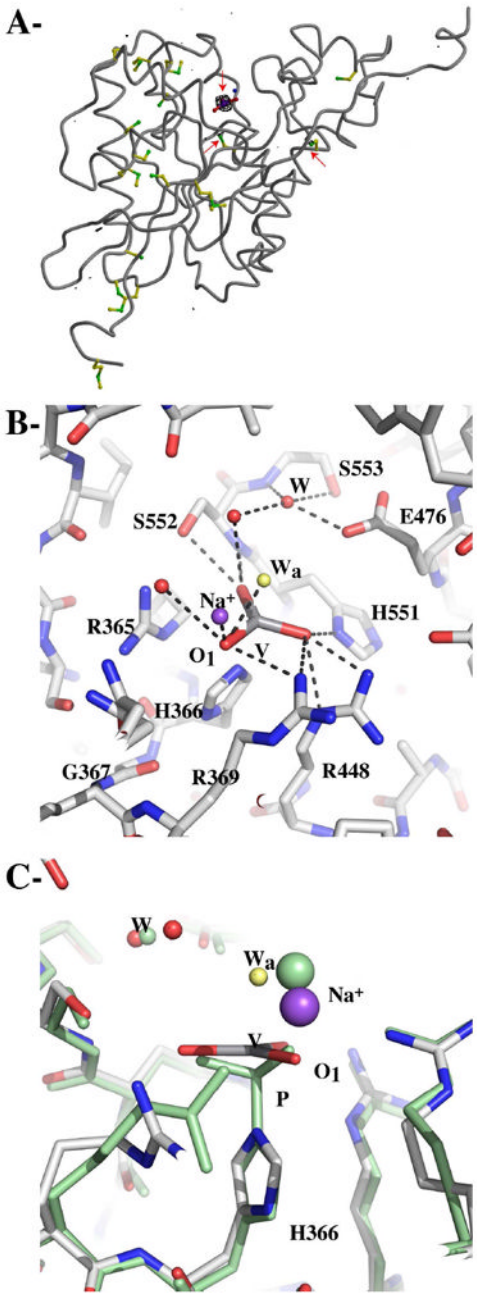


**Figure 2.**

Structure of $VO_3$-bound Sts-$2_{PGM}$. **A**- An anomalous difference Fourier electron density map is represented at +4σ cutoff and overlaid over one Sts-$2_{PGM}$ monomer. Positive peaks (highlighted by red arrows) superpose over the vanadium and the sulfur of two Cys residues. For simplicity, only the Cys and Met residues are shown in ball-and-stick representation. **B**- Putative interactions made by the $VO_3$ molecule and active site residues of Sts-$2_{PGM}$ or solvent molecules are shown as dotted lines. The apical water ($W_a$) that sits on top of the $VO_3$ molecule and completes the pentavalent coordination of the vanadium atom is shown as a yellow sphere. The possible candidate for the nucleophilic water molecule is labeled with a W. Its interactions with the protein are also shown as dotted lines. **C**- Superposition of the structures of

NIH-PA Author Manuscript

NIH-PA Author Manuscript

NIH-PA Author Manuscript

phosphorylated (light green) and $VO_3$-bound Sts-$2_{PGM}$ around His366 shows that the V-NE2 bond is longer than the V-P covalent bond.

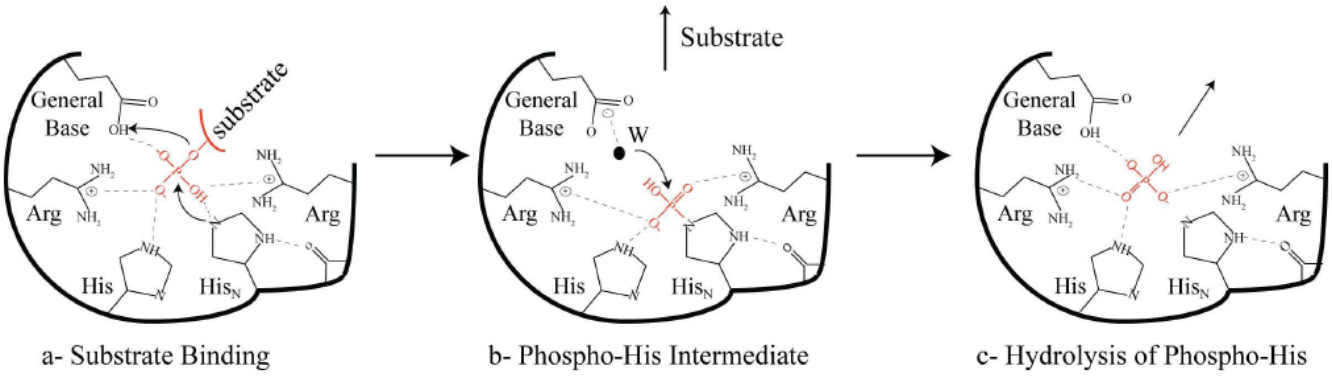


**Scheme.**

Schematic representation of the phosphatase reaction catalyzed by 2H-phosphatase family members. Only drawn are the conserved active site residues. The phosphorylated substrate binds to the active site such that the phosphorus atom is within an attacking distance from the nucleophilic His ($His_N$) (*a*). The phosphate is then transferred to $His_N$ to generate the phosphorylated intermediate and the dephosphorylated substrate is released (*b*). Phospho-$His_N$ is next hydrolyzed by a nucleophilic water molecule (W) that is activated by a general base and the phosphate is released into the solvent (*c*). Dotted lines represent hydrogen-bond interactions.



NIH-PA Author Manuscript NIH-PA Author Manuscript NIH-PA Author Manuscript

NIH-PA Author Manuscript
NIH-PA Author Manuscript
NIH-PA Author Manuscript



## Table 1

Statistics on Crystallographic Data Collection and Model Refinement.

| | $VO_3$ | phospho-His366 |
|---|---|---|
| **Data Collection** | | |
| Resolution (Å) | 50.0 - 1.86 | 50.0 - 2.05 |
| Number of Unique Reflections | 90,022 | 68,508 |
| Completeness, overall (last resolution shell)† (%) | 99.9 (100.0) | 98.8 (96.6) |
| Redundancy, overall (last resolution shell)† | 7.1 (6.2) | 6.3 (6.1) |
| $\langle I \rangle / \langle \sigma(I) \rangle$, overall (last resolution shell) † | 32.5 (2.6) | 22.6 (2.9) |
| $R_{sym}$* (%) | 5.8 (67.5) | 7.3 (56.0) |
| **Model Refinement** | | |
| N° of reflections used in refinement | 85,379 | 64,807 |
| $R_{free}$†, (%) overall (last resolution shell) | 24.0 (26.5) | 27.0 (31.4) |
| $R_{work}$‡, (%) overall (last resolution shell) | 20.2 (24.0) | 21.8 (22.3) |
| $R_{cryst}$‡‡, (%) | 20.4 | 22.1 |
| rms deviation in bond length, (Å) | 0.013 | 0.013 |
| rms deviation in bond angle, (°) | 1.413 | 1.520 |
| Estimated standard uncertainties§, (Å) | 0.148 | 0.209 |
| Ramachandran plane¶, (%) | 92.0/8.0 | 90.6/9.4 |
| N° of non-hydrogen atoms used in refinement | 8,906 | 8,822 |

† last shell is 1.93 – 1.86 and 2.12 – 2.05 Å for the VO3 and phospho-H366 data, respectively.

* $R_{sym} = \Sigma_{i,\,hkl} |\langle I(hkl) \rangle - I_i(hkl)| / \Sigma_{i,\,hkl} I_i(hkl)$

† $R_{free} = \Sigma(hkl) \varepsilon T ||F_{obs}| - |F_{calc}|| / \Sigma(hkl) \varepsilon T |F_{obs}|$, where T is the test set (23) obtained by randomly selecting 5% of the data.

‡ $R_{work} = \Sigma(hkl) \varepsilon W ||F_{obs}| - |F_{calc}|| / \Sigma(hkl) \varepsilon W |F_{obs}|$, where W is the working set.

‡‡ $R_{cryst} = \Sigma(hkl) ||F_{obs}| - |F_{calc}|| / \Sigma(hkl) |F_{obs}|$ calculated over the entire set of unique reflections.

§ e.s.u. calculated from $R_{free}$ statistics.

¶ Most favored/additional allowed regions.